Multi-Megahertz IPT Systems for Biomedical Devices Applications

Nunzio Pucci, Christopher H. Kwan, David C. Yates, Paul D. Mitcheson
Department of Electrical and Electronic Engineering, Imperial College London, United Kingdom

Abstract

This paper investigates the main design constraints for the optimisation of an inductive power transfer (IPT) link for recharging implantable medical devices [1], and presents the potential advantages of operating in the multi-MHz range for such applications. The design proposed in this paper offers a fast charging solution, allowing patients to recharge their active medical implants every 4-5 years for 40% of its battery capability. The main challenge consists of obtaining good coupling and effective Q factor of the receiver coil, while minimizing the overall increase in size of the medical implant. Analysis obtained through electromagnetic simulations with CST Studio Suite for a 13.56 MHz, 1 W system suggests that it is possible to achieve a relatively high theoretical link efficiency of 66%, while keeping surface temperature increases and specific absorption rate (SAR) within the limits established in EN 45502 [2] and ICNIRP 1998 [3]. The experimental results show two feasible systems with different separation distances between the device's metallic case and the receiver coil, achieving transfer efficiencies [11] of 41% and 53% for separations of 1 mm and 7 mm, respectively.

Introduction

The most significant benefit of a wirelessly-recharged implantable device lies in the reduction of potential risks derived from surgery procedures for battery replacement every 3-15 years. There are several examples of wireless power transfer systems for medical implants that operate at frequencies in the kHz range or at 100s of MHz. The 403 MHz, 61 mW system presented in [5] would result in very long charge times due to the low amount of power transferred (mainly limited by the high SAR achieved at that specific frequency). In [6], a 20 kHz solution achieved a link efficiency of 72%, but the separation distance between the coils was optimistically set to 1.5 cm; further biocompatibility problems might arise due to the required ferrite plate in the implantable device.

This paper presents the advantages of operating an IPT system in the multi-MHz range in order to enable the fast and safe charging of implantable medical devices. Two 13.56 MHz systems were built and tested, following a design process that considers the effect of the surrounding environment (biological tissue and metallic device body) on the magnetic link. The systems consist of two planar FR4, two-turn coils for the transmitter and the receiver (with a 4 cm spacing for a tissue-simulating phantom comprising a layer of agarose gel at a fixed salinity of 10%), a class EF inverter on the transmitter side and a class D rectifier on the receiver side.

The experimental setup needs to emulate the mutual coupling between a receiver coil and the titanium case of a device [4]: the first proof-of-concept 'Initial Prototype' uses a folded aluminium sheet with a 7 mm separation from the receiver coil. The second 'Compact System' uses an actual pacemaker device with a smaller separation from the receiver coil (1 mm), making this a smaller and easier-to-implant version of the 'Initial Prototype'. The 'Compact System' is a much more accurate representation of a realistic scenario, addressing much stricter size and placement constraints and the results are visible in terms of transfer efficiency.

For both systems, the SAR was below the 2 W/kg limit for general public exposure in [3] and the measured temperature increase of the system was not higher than 1° C. In summary, a high level of power transfer was achieved without exceeding the applicable limits in [2] and [3], thus providing a viable alternative solution to what is presented in [5] and [6].

Optimization of the Inductive Link

The design problem to be addressed is the optimisation of link efficiency of an IPT system in the presence of its surrounding materials. Within the context of medical implants, the wireless power system is situated in an environment consisting of biological tissue between the transmitter and the receiver coils, and a titanium block of approximately 5cm x 5cm x 1.5cm (representing the implantable device body) placed behind the receiver coil as shown in Fig. 4(b). As explained in [4], the presence of a titanium case can be potentially detrimental to link efficiency. Further investigation through CST Studio Suite simulations showed that while the biological tissue contributed to a decrease in efficiency of up to 9%, the device's titanium body caused an efficiency drop of 11% with a separation distance of 7 mm between the receiver coil and the device's case. If the separation is reduced to 1 mm, efficiency decreases by 45% instead.

Maximum achievable link efficiency, η_{link}^{max}, can be derived as shown in [10] and is illustrated in Equation 1.

The parameters determining this value are coupling factor, *k* (mainly dependent on position and geometry of the coils but also affected by the titanium body), and the quality factors of the receiver and transmitter coils, Q_{RX} and Q_{TX}, respectively. A decrease in any of these three variables can cause a decrease in link efficiency.

$$\eta_{link}^{max} = \frac{k^2 Q_{RX} Q_{TX}}{(1+\sqrt{1+k^2 Q_{RX} Q_{TX}})^2}$$

Equation 1

Equations 2 and 3, obtained from [4], illustrate how the presence of the biomedical device affects link efficiency, by modelling the titanium body as a third coupled coil in the system (where Z_{ref} is the reflected impedance, $M_{RX\text{-}C}$ is the mutual inductance between the receiver coil and the titanium body, ω is the angular operating frequency, L_C and R_C are the effective inductance and resistance of the titanium body, L_{RX} and R_{RX} are the effective inductance and resistance of the receiver coil, and $Q_{RX\text{-}eq}$ is the effective quality factor of the receiver coil in situ). The reflected impedance [7] from the titanium body causes a decrease in the receiver coil's equivalent quality factor, hence lowering the link efficiency. It is important to keep in mind that the equivalent quality factor of the receiver coil also varies with separation between the receiver coil and the biomedical device: as the separation distance decreases, the coupling between the receiver coil and the equivalent model of the titanium case increases, further increasing reflected impedance and lowering link efficiency.

$$Z_{ref} = \frac{M_{RX-C}^2 \omega^2 R_C}{(\omega L_C)^2 + R_C^2} - j\frac{M_{RX-C}^2 \omega^3 L_C}{(\omega L_C)^2 + R_C^2}$$

Equation 2

$$Q_{RX-eq} = \frac{\omega L_{RX} - Im(Z_{ref})}{R_{RX} + Re(Z_{ref})}$$

Equation 3

The main design choices then lie in optimising for the quality factor of the receiver coil and for the mutual coupling between the transmitter and receiver while maintaining a minimum distance between the implantable medical device and the receiver coil. For a feasible solution it is also necessary to have a coil dimension that does not exceed that of the implantable device: for this reason the size of the PCB coil was kept to 50mm x 50mm x 2mm in the 'Initial Prototype', and lowered to 40mm x 40mm x 0.6mm in the final 'Compact System'.

The first optimisation step is to identify the optimal number of turns for the two coils. Despite the trace thickness and planar coil geometry affecting both coupling and quality factor, their influence is relatively small when compared to variations in coil-turns. As shown in Fig. 1, despite maximum coupling being obtained for 3 turns on both transmitter and receiver coils, the highest link efficiency is obtained for 2 turns on each coil, meaning that for the 3-turn case the decrease in the product $Q_{RX}Q_{TX}$ was more significant than the increase in k^2.

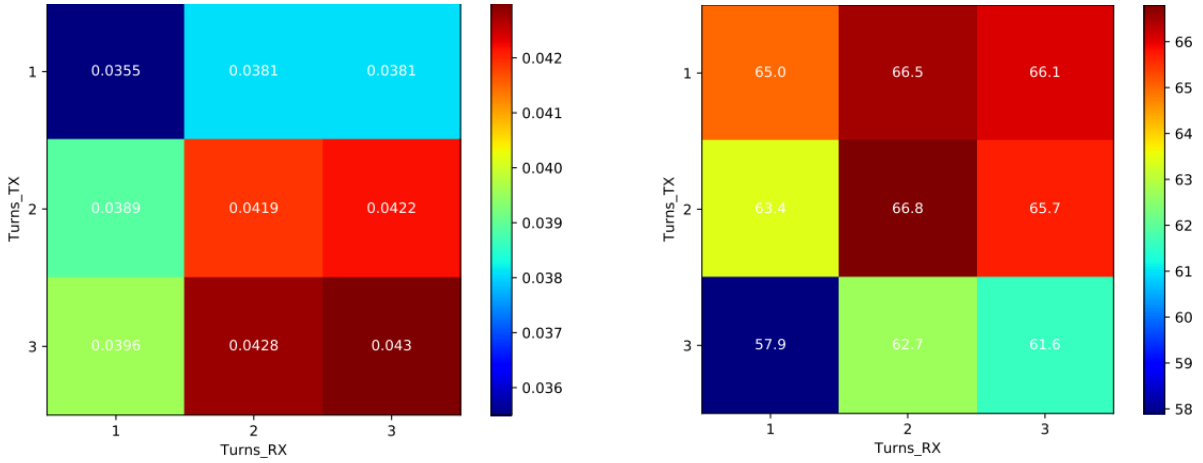

(a) Variation of coupling factor with number of turns

(b) Variation of maximum link efficiency (%) with number of turns

Fig. 1. Optimisation of coil turns

The second optimization step is the selection of the operating frequency. From Fig. 2 it is possible to observe that the quality factor of the receiver coil is shaped by two effects: the low frequency portion is dominated by skin effect ($Q\alpha\omega^{1/2}$) and the high frequency portion is dominated by radiation ($Q\alpha\frac{1}{\omega^3}$). The transition point between these two yields a quality factor maximization point, resulting in an optimal frequency.

With a preference to operate within the ISM bands, the possible frequencies to use are 6.78 MHz, 13.56 MHz and 27.12 MHz. It is visible from Fig. 2 that this maximization point shifts as the separation distance between the receiver coil and device case varies. The graph suggests that the 10 MHz to 20 MHz frequency range contains the maximization points for all the feasible separation values considered. This leads to the choice of an operating frequency of 13.56 MHz (although in different setups with lower distance and smaller coils, an operating frequency of 27.12 MHz might be preferable).

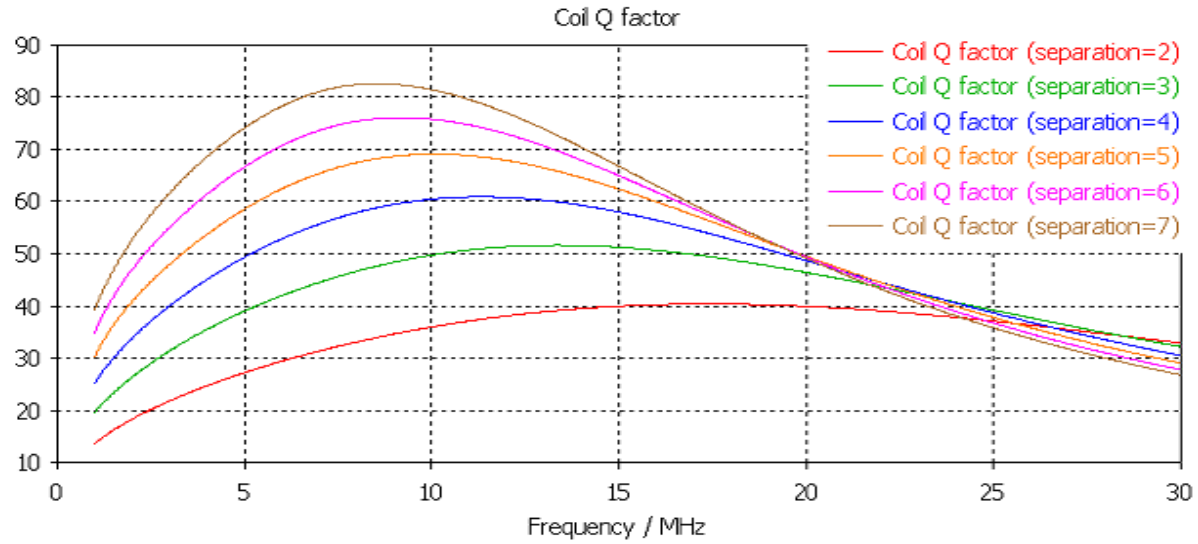

Fig. 2. Variation of quality factor of receiver coil with frequency

Circuit Architecture

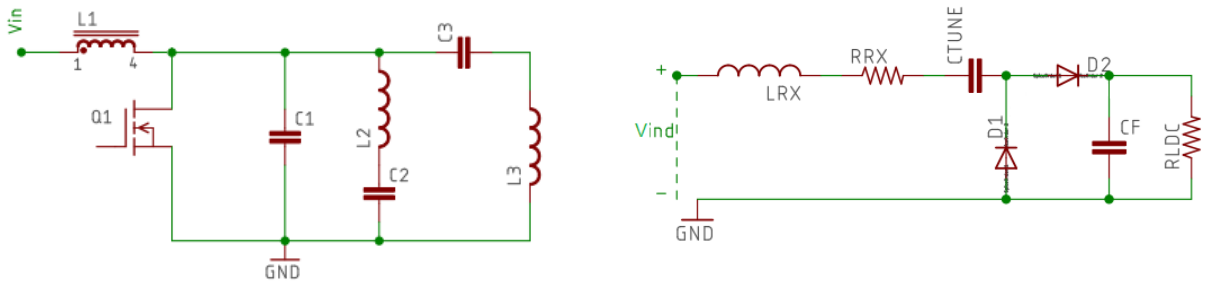

(a) Class EF Inverter (b) Half-wave Class D rectifier

Fig. 3. IPT system circuit schematic

One of the most challenging aspects in the design of an IPT system with small coils and little control on their precise alignment is the change in coupling factor. This aspect can heavily affect efficient operation of the power electronics on the transmitter side. The advantages of using a load independent inverter circuit have been widely discussed in [8], where the effect of variation in coupling factor on overall system efficiency is minimized through the use of a load independent class EF inverter. The system presented in this paper uses the same circuit topology. The main design criteria for the receiver side are size and circuit simplicity. The rectifier topology chosen was a half-wave class D as shown in Fig. 3. The 'Initial Prototype' version used an external PCB connected perpendicularly to the receiver coil (Fig. 4(a)) to minimize coupling between the coil and possible signal paths on the board. Since there was no observed coupling issues, the rectifier was later integrated on the bottom of the planar coil as shown in Fig. 5(b) for the final 'Compact System', making the receiver system smaller and more suitable for implantation.

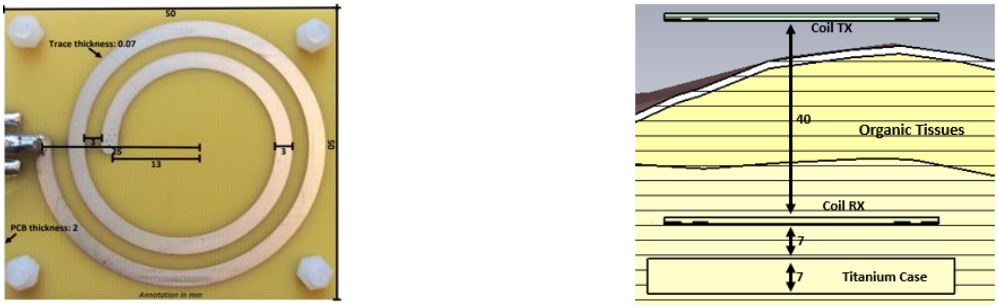

(a) Coil for TX in both systems, and RX in 'Initial Prototype' (b) Implanted system in the human body model

Fig. 4. Implanted system dimensions (mm)

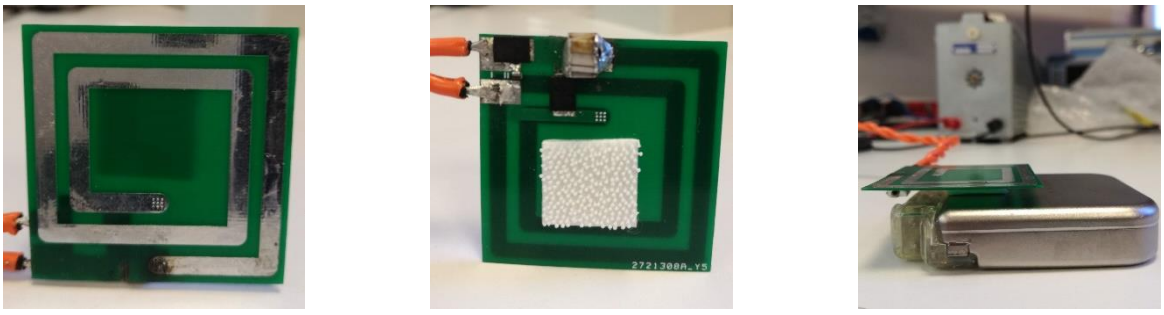

(a) Top view (b) Bottom view (c) Assembled system

Fig. 5. RX coil with 1 mm separation from implantable device in the final 'Compact System'

Experimental Results

The experimental work focused on the characterization of the transfer efficiency [11] of the 'Initial Prototype', measurement of the peak efficiency of the final 'Compact System' for ideal alignment conditions, and recording the temperature variation of the two systems.

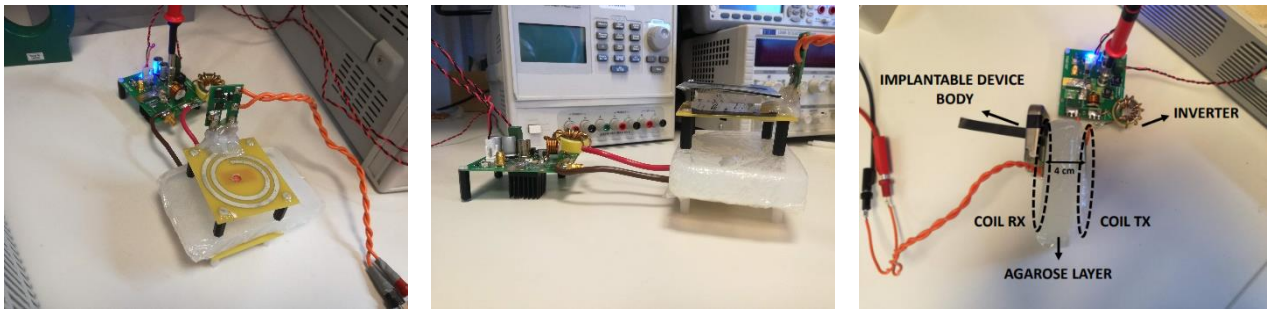

(a) Initial Prototype' tested with agarose layer

(b) 'Initial Prototype' tested with agarose layer and aluminum Sheet

(c) 'Compact System' tested with agarose layer and implantable device

Fig. 6. Test setup of both the 'Initial Prototype' and 'Compact System'.

The first characterization test showed similar results to what was obtained in CST Studio Suite simulations. The theoretical optimal load, found by Equation 4 [10], matched the experimental findings at around 7.4 **Ω**. An increase in optimal load value was observed as the receiver coil's equivalent quality factor and coupling factor started to drop, as highlighted in the three cases presented in Fig. 7. This may be explained as a faster decrease in Q_{RX} in comparison with k.

$$R_{opt} = \omega L_{RX}\left(\frac{\sqrt{1+k^2 Q_{TX} Q_{RX}}}{Q_{RX}}\right)$$

Equation 4

During this characterization test the distance between the two coils was kept at 4 cm, with a 2.5 cm thick agarose layer interposed between the coils. As shown in Fig. 6b, the 'Initial Prototype' system operated with a folded aluminium sheet placed at a distance of 7 mm from the receiver coil. Under these operating conditions, the peak efficiency reached 53%.

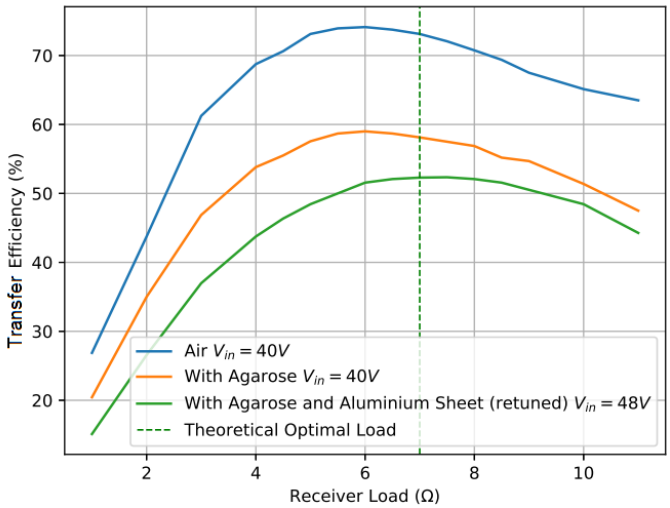

Fig. 7. Variation of transfer efficiency (%) with receiver load in different scenarios

In the 'Compact System' setup (Fig. 6(c)) the separation between coils was optimized with the aim of replicating a more realistic scenario: the agarose layer's thickness was increased to 4 cm, filling the previous 1.5 cm airgap. As shown in Fig. 5(c) the separation between the device and the receiver coil is extremely small (1 mm). The optimal load was again found to be close to the predicted value at 1.5 **Ω** and the system achieved a transfer efficiency of 41%.

As explained in [1], low link efficiencies may lead to both heating of the biological tissue and an increase in localized SAR in specific areas of the body. As it was not possible to obtain a direct measurement for SAR, the only feasible test for patient's safety was a measurement of temperature variation of the two systems before and after running them over a period of time. Fig. 8 illustrates the heating of the components of the 'Initial

Prototype' after 10 minutes of operation. It is possible to observe that the temperature of the implanted components does not rise by more than 1°C from their initial temperature, complying with [2]. However, further investigation in a temperature-controlled environment will be required in the future. The temperature variation in the components of the 'Compact System' led to the same conclusions. It is possible to observe coherence with the simulated results in Fig. 9, obtained from thermal simulations in CST Studio Suite.

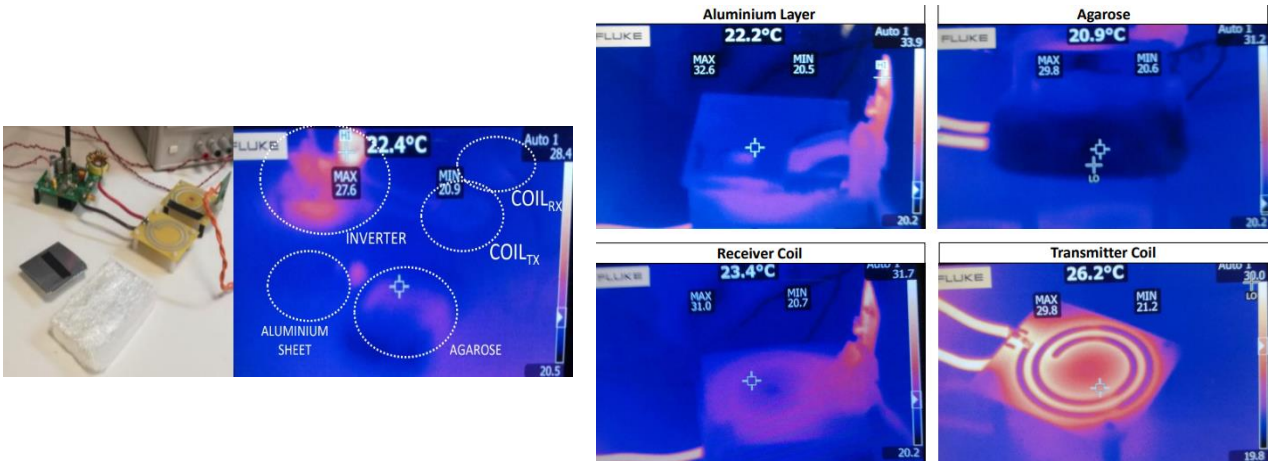

(a) Temperatures before Operation (b) Temperatures after 10 minutes of operation

Fig. 8. Temperature of various components of 'Initial Prototype' system before and after 10-minute operation

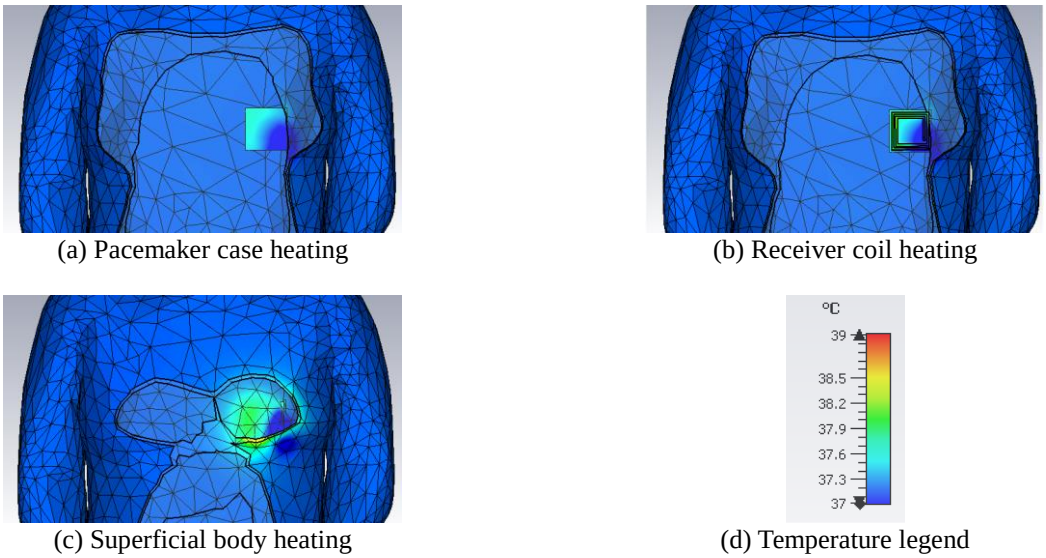

(a) Pacemaker case heating (b) Receiver coil heating

(c) Superficial body heating (d) Temperature legend

Fig. 9. Simulated temperature distribution of the implanted wireless charging system

The energy absorption in biological tissue is regulated by ICNIRP 1998 [3], which gives a SAR limit of 2 W/kg for general public exposure averaged over 10 g of contiguous organic tissue over any six-minute period. The two different systems do not exceed the limit as shown from electromagnetic simulations in Fig. 10. A direct comparison between (a) and (b) in Fig. 10 shows a significant difference in the main region of heat accumulation, with case (a) showing a peak under the epidermal and adipose layers, while din case (b) most of the energy is accumulated in the superficial layers. This is ultimately expected due to the higher amount of transmitter coil's current in (b) for optimal load conditions when the system is operating at lower coupling and with a lower receiver coil equivalent quality factor.

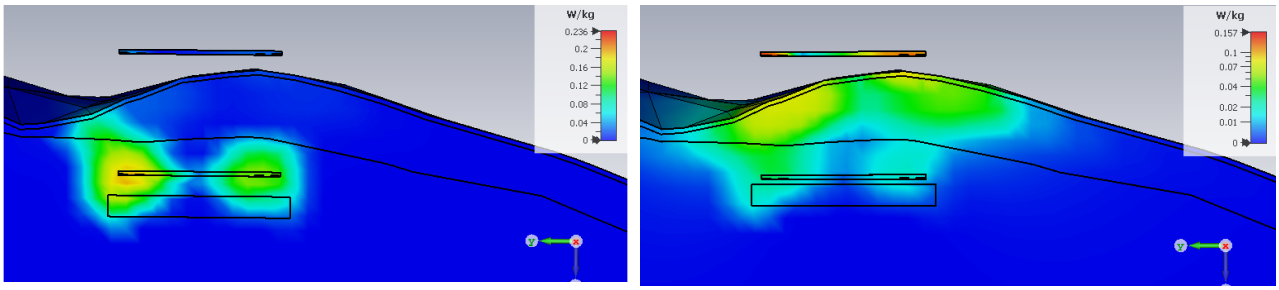

(a) 7 mm separation from pacemaker body (b) 1 mm separation from pacemaker body

Fig. 10. CST-simulated SAR distribution

Further safety investigation will be needed in the future, analysing in depth possible interactions between the implantable biomedical device and the generated high-frequency magnetic field, adopting a similar approach to what is suggested in [9] and obtaining a more complete assessment of all the quantifiable risks that a patient would be subjected to.

Summary

This paper showed the feasibility of wirelessly-rechargeable implantable biomedical devices for a power level of 1 W through a compact IPT system in close proximity to the device's metallic body. The system showed conformity with SAR limits in ICNIRP 1998 and surface temperature increase limits in EN 45502, indicating promising results for an early stage safety assessment of this emerging technology. Despite the requirement for further testing to prove safety of the implanted system, this paper highlighted the main benefits granted by multi-MHz frequency operation of IPT systems in the field of implantable medical devices, illustrating some the main design challenges linked with the interaction between a wireless power link and the surrounding materials.

Acknowledgements

The authors would like to acknowledge the following funding sources: EPSRC Departmental Funding - Imperial College Department of Electrical and Electronic Engineering 2019

References

[1] C. H. Kwan, D. C. Yates, and P. D. Mitcheson, Design objectives and power limitations of human implantable wireless power transfer systems, 2016.
[2] BSI, BS EN 45502-1:2015, Implants for surgery. Active implantable medical devices. General requirements for safety, marking and for information to be provided by the manufacturer, Jun. 2015.
[3] ICNIRP, Guidelines for limiting exposure to time-varying electric, magnetic and electromagnetic fields (up to 300 GHZ), 1998.
[4] P. Pérez-Nicoli, M. Biancheri-Astier, A. Diet, Y. Le Bihan, L. Pichon, and F. Silveira, "Influence of the titanium case used in implantable medical devices on the wireless power link", Jun. 2018, pp. 1–3. doi: 10.1109/WPT.2018. 8639416.
[5] Giuseppina Monti, Maria Valeria De Paolis, Laura Corchia, Luciano Tarricone, Mauro Mongiardo, Wireless Power Link for Rechargeable Pacemakers, 2017.
[6] Vladimir Vulfin, Shai Sayfan Altmanban, Reuven Ianconescu, Wireless power transfer for a pacemaker application, 2018.
[7] K. Finkenzeller, RFID-Handbook, 2nd ed. Hoboken, NJ: Wiley, 2003
[8] J. M. Arteaga, S. Aldhaher, G. Kkelis, C. Kwan, D. C. Yates and P. D. Mitcheson, "Dynamic Capabilities of Multi-MHz Inductive Power Transfer Systems Demonstrated With Batteryless Drones," in *IEEE Transactions on Power Electronics*, vol. 34, no. 6, pp. 5093-5104, June 2019.
[9] N. Pucci, C. H. Kwan, D. C. Yates, A. D. Arnold, D. Keene, Z. I. Whinnett, P. D. Mitcheson, "Effect of Fields Generated Through Wireless Power Transfer on Implantable Biomedical Devices,"
[10] K. van Schuylenbergh and R. Puers, Inductive Powering, Basic Theory and Application to Biomedical Systems. Springer, 2009.
[11] M. Pinuela, D. C. Yates, S. Lucyszyn and P. D. Mitcheson, "Maximizing DC-to-Load Efficiency for Inductive Power Transfer," in IEEE Transactions on Power Electronics, vol. 28, no. 5, pp. 2437-2447, May 2013

Corresponding author: Nunzio Pucci, Imperial College London, South Kensington Campus, SW7 2AZ, London, UK, +447783822055, nunzio.pucci15@imperial.ac.uk